Model Predictive Control Based Integral Line-of-Sight Curved Path Following for Unmanned Aerial Vehicle

Conference Paper · January 2017

DOI: 10.2514/6.2017-1511

CITATIONS
3

READS
198

4 authors, including:

Shulong Zhao
National University of Defense Technology
26 PUBLICATIONS **79** CITATIONS

SEE PROFILE

Xiangke Wang
National University of Defense Technology
94 PUBLICATIONS **782** CITATIONS

SEE PROFILE

Model Predictive Control Based Integral Line-of-Sight Curved Path Following for Unmanned Aerial Vehicle

Shulong Zhao*, Xiangke Wang , Daibing Zhang and Lincheng Shen*

National University of Defense Technology, Changsha, 410073, P. R. China.

This paper develops a novel three-dimensional (3D) curved path following strategy that combines integral line-of-sight (LOS) guidance logic and model predictive control (MPC) approach to ensure a small fixed-wing unmanned aerial vehicle (UAV) converging to the followed curved path with input constraints. On one hand, we need robust control laws in the low level layer to stabilize the vehicle and track references (such as airspeed, desired attitude, etc.), which must be implemented safely in the overall flight envelopes. On the other hand, we need accurate guidance logics in the high level layer to steer the vehicle converging to a predefined path to fulfill the missions. However, most guidance logics implemented to follow the desired geometrical path and control schemes employed to minimize the cross track error are designed separately. To obtain a combination of fast convergence and minor overshoot compared with the LOS algorithm with a constant lookahead distance, a modified MPC scheme integrated with the integral LOS guidance logic is proposed to generate an optimal lookahead distance along the error model of the UAV, which is defined in Frenet-Serret frame with control constraints considered explicitly. Reasonable decision of the lookahead distance is incorporated into the MPC design process and quadratic programming (QP) method is employed to solve the problem of MPC. Curved path following performances of the vehicle with fixed and variable lookahead distances are provided in high-fidelity semi-physical experiments to illustrate the effectiveness and applicability of the proposed control strategy.

Nomenclature

$\mathbf{q}$	Position of the UAV, m
V_a	Airspeed, m/s
V_g	Groundspeed, m/s
W	Wind speed, m/s
g	Gravity acceleration, m/s^{-2}
ϕ_c	Command roll angle, degree
α	response coefficient of flight path angle
γ_c	Command path angle, degree
χ	Course angle, degree
γ	Flight path angle, degree
ψ	Heading angle, degree
R_I^F	Rotation matrix
χ_p	Path course angle, degree
$\omega_{F/I}$	Angle rate of the UAV, degree/s
s	Arc-length parameter
Δ	Lookahead distance, m
T_s	Sampling time, s

I. Introduction

Recently, the interest in the problem of curved path following control for fixed-wing unmanned aerial vehicles (UAVs) has significantly increased.[1,2] Two types of algorithms for path following exist, as follows: (1) geometry-

*Dr. Zhao, with College of Mechanics and Automation, National University of Defense Technology, Changsha, P. R. China, email: jaymaths@nudt.edu.cn.

based algorithms and (2) dynamic-based algorithms. The geometry-based method emphasizes the geometry relations between a desired path and the aircraft, and a control strategy is developed with positions and heading angles, such as pure pursuit guidance[3] and position feedback control.[4] The dynamic-based method, which is a model based control design technique, considers the dynamic characteristics of aircraft and employs navigation control command by the out-loop of autopilot, such as the theory of nested saturations,[5] adaptive backstepping[6] and vector field (VF) method.[7] A common assumption of those two algorithms is the existence of a proper inner-loop of the autopilot.

Once the desired path is planned, the objective of most path following methods is to enable a UAV to track the desired path and attain a tolerable error range. Unlike the problem of trajectory following, the curved path is not parameterized by time and information about the desired path can be obtained in advance.[8] The UAV must be move near the path, but the time parameterizations of the path may not be critical. A basic capability for path following methods is accurate and robust to wind disturbances.[9] For the majority of miniature UAVs with the path following problem in a two-dimensional plane(x, y), the movement characteristics are similar to a wheel robot or a unicycle vehicle.

In most path following strategies, the desired path usually consists of straight-line or loiter and attentions are rarely given to general curved path. In the mission of obstacle avoidance, search and surveillance, the vehicle guides itself in a manner in which it passes through a curved path that is convenient and practical to fulfill a desired purpose. In actual flight applications, curved path following is commonly achieved because it is practical and available for every vehicle. Control over vehicle position for curved path following is distinguished from a straight line or loiter path, and the path may be combined with a line and loiter. The properties of the path must be considered, and sufficient and rapid reduction of the tracking error is also required. In addition, the initial state of the vehicle is important for developing a proper guidance scheme.

In recent years, the guidance logic based on the Line-of-Sight (LOS) method is used extensively for small fixed-wing UAVs. The idea of the LOS guidance embodies an intuitive considering of the performance of the UAV and the operation of a pilot. A desired LOS angle is generated by the combination of the cross tracking error and a lookahead distance Δ, which is a predefined parameter used to decide the convergence of the UAV to the desired path tangential. The LOS guidance logic is a well documented strategy for path following and it ensures that the angle between the UAV and a ghost vehicle that follows the desired path is the same as that of the LOS angle. However, it is very difficult to consider a proper lookahead distance Δ in realistic implementations and the performance of the control scheme will be limited by a constant Δ. There is a tradeoff that large Δ will lead to rapid convergence and oscillations when the tracking error approaches to zero, and small Δ will cause slow convergence and the UAV may lose efficacy in some extreme circumstances. This behavior is natural for a UAV since locally Δ corresponds to the inverse proportional gain of the desired LOS angle.

A LOS guidance logic is employed for path following of a low cost autonomous vehicle,[10] and the sideslip angle of the vehicle is ignored, which limits the path following performances of the UAV when gust wind appears. Zheng utilizes sensors of velocities to measure the sideslip angle, and the effect of sideslip is compensated simultaneously.[11] In fact, the sensors are expensive and they are easily polluted by noise, which may generate large tracking error and oscillations during path following. Aiming at eliminating the effect of sideslip, an integral LOS guidance is proposed originally,[12] and the system dynamics are presented with absolute velocities, which requires an additional adaptive scheme to compensate unknown disturbances. A modified integral LOS guidance with feedback controllers is introduced[13] and the model of the vehicle is expressed with relative velocities to cancel the adaptive scheme. In Ref,[14] the Δ of a LOS guidance is embedded in the linear Model Predictive Control (MPC) controller design as an additional decision to obtain a fast convergence and small overshoot performance of the UAV.

However, only straight line is considered as the desired path of those studies.[10–14] An integral LOS path following approach is developed[15] for continuous curved path, which is locally interpolated by cubic hermite spline method through all predefined waypoints (WPs) and it is able to expand with new added WPs. The issue of compensating for sideslip angle is emphasised and the stability of the integral LOS method is illustrated explicitly. A cascaded scheme of LOS guidance and adaptive sliding mode controller is proposed for path following to compensate drift force[16] and the desired path is curved path with constant curvature.

Meanwhile, the output of a controller is often limited due to constraints on inputs and states in actual flight applications. The MPC method is the most widely employed control approach because it offers, through the receding horizon implementation, an eminently sensible compromise between optimality and speed of computation. The MPC method solves a constrained optimization problem repetitively online in a receding horizon way and one of the main reasons for the success of the MPC method is that its ability to explicitly take constraints into account.

We propose a novel curved path following strategy that combines the integral LOS guidance logic and an MPC appraoch to ensure a small fixed-wing UAV converging to the desired curved path with input constraints. The main

contributions of this study are summarized as follows.

1. To achieve the optimal performance of curved path following for a fixed-wing UAV in three-dimensional (3D) space, the lookahead distance Δ of an integral LOS approach is selected to be time-varying and optimized in the process of an MPC designation. The effect of wind disturbances that drives the vehicle away from the desired path has been significant canceled.

2. The proposed method is implemented with online optimization, which provides faster convergence and smaller overshoot than what can be achieved with a constant Δ as is employed in existing integral LOS guidance in,[13,14] thus can be practical in real-time applications.

3. High-fidelity semi-physical experiments are provided to illustrate the effectiveness and applicability of the proposed control strategy. The solution has a sufficient real-world scenario and can be directly applied to flight experiments with minor adjustments.

To our knowledge, while the LOS guidance scheme has been reported for small fixed-wing UAV applications,[11,15,16] approaches on the MPC scheme integrated with the LOS guidance for small fixed-wing UAV curved path following under control constraints have not been seen in open literature to date.

The rest of the paper is organized as follows. In Section II, we summarized the primary introduction of the tracking error equation and some necessary notations. Then we involve a proper MPC scheme for tracking error system with the input constrained case, and a reasonable decision of the lookahead distance to satisfy the constraint condition is explained in Section III. Experiment results are reported in Section IV and some concluding remarks are provided in Section V.

II. Background and Problem Statement

A. Model of the UAV

In this section, a planar model of the UAV is employed to perform coordinated flight.[5]

$$\begin{aligned} \dot{x} &= V_a \cos\psi \cos\gamma + W_x = V_g \cos\chi \cos\gamma \\ \dot{y} &= V_a \sin\psi \cos\gamma + W_y = V_g \sin\chi \cos\gamma \\ \dot{z} &= -V_a \sin\gamma + W_z = -V_g \sin\gamma \\ \dot{\chi} &= \Gamma(\psi)\frac{g}{V_g}\tan\phi_c \\ \dot{\gamma} &= \alpha(\gamma_c - \gamma) \end{aligned} \tag{1}$$

where, $\Gamma(\psi) = \frac{V_a^2 + V_a(W_x\cos\psi + W_y\sin\psi)}{V_a^2 + W_x^2 + W_y^2 + 2V_a(W_x\cos\psi + W_y\sin\psi)}$.

The position of the UAV is $\mathbf{q} = (x, y, z)$, V_a and V_g are airspeed and groundspeed of the UAV, respectively. $W = (W_x, W_y, W_z)$ is wind speed. g is the gravity acceleration. ϕ_c is the command roll angle. α is the response coefficient of flight path angle. γ_c is the command flight path angle. In the field of path following, this model is widely utilized and it is suitable to describe the navigation kinematic of most common distributed fixed-wing UAVs equipped with a propeller and a set of control surfaces (elevator, ailerons, and rudder).

The coordinates of the UAV including the world frame, {I}, body frame, {B}, and Frenet-Serret frame, {F}, can be described in Fig. 1. The blue dotted line indicates the desired path, and we define vector $\mathbf{q} = \overrightarrow{OQ}$, $\mathbf{P} = \overrightarrow{OP}$, $\mathbf{r} = \overrightarrow{QP}$. The direction of the ground speed vector V_g relative to the inertial frame {I} is specified using two angles, the course angle χ and the flight path angle γ.

γ is defined as the angle between the lateral plane and the ground velocity vector, ψ represents heading angle of a UAV and it is the direction that the UAV is pointed. Course is the direction of travel relative to the earth's surface. In the absence of wind, the crab angle, the difference between χ and ψ, is zero.

B. Frenet-Serret frame

Here, we use the Frenet-Serret[8] frame to define the reference path, which is represented by arc-length parameter s. The x-axis of the Frenet-Serret frame is aligned with the tangent vector to the path.

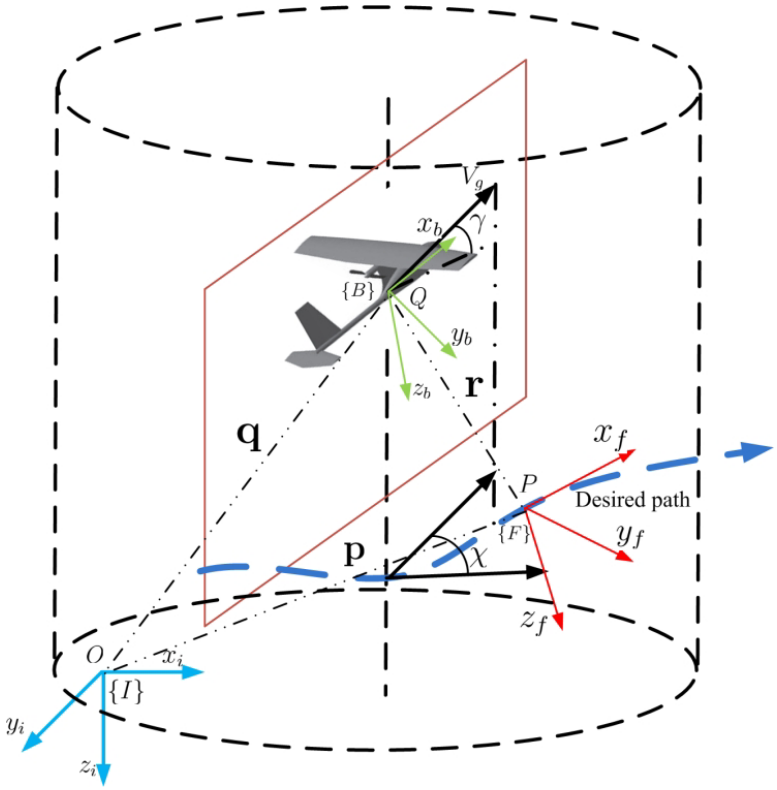

Figure 1. The coordinates of the UAV

We define

$$R_I^F = \begin{pmatrix} \cos\gamma_p & 0 & -\sin\gamma_p \\ 0 & 1 & 0 \\ \sin\gamma_p & 0 & \cos\gamma_p \end{pmatrix} \begin{pmatrix} \cos\chi_p & \sin\chi_p & 0 \\ -\sin\chi_P & \cos\chi_p & 0 \\ 0 & 0 & 1 \end{pmatrix} = \begin{pmatrix} \cos\gamma_p\cos\chi_p & \cos\gamma_p\sin\chi_p & -\sin\gamma_p \\ -\sin\chi_p & \cos\chi_p & 0 \\ \sin\gamma_p\cos\chi_p & \sin\gamma_p\sin\chi_p & \cos\gamma_p \end{pmatrix} \tag{2}$$

is the rotation matrix from the the inertial frame to Frenet-Serret frame. γ_p and χ_p are locally defined as follows.

$$\chi_p = \tan^{-1}\left(\frac{y_f(s)}{x_f(s)}\right) \tag{3}$$

$$\gamma_p = \tan^{-1}\left(\frac{z_f(s)}{\sqrt{x_f(s)^2 + y_f(s)^2}}\right) \tag{4}$$

Then we can define

$$\dot{\chi}_p = \frac{d\chi_p}{ds}\frac{ds}{dt} = \alpha(s)\dot{s} \tag{5}$$

$$\dot{\gamma}_p = \frac{d\gamma_p}{ds}\frac{ds}{dt} = \beta(s)\dot{s} \tag{6}$$

The angle rate of the UAV on the path can be expressed as

$$\omega_{F/I} = \begin{pmatrix} 0 \\ \dot{\gamma}_p \\ 0 \end{pmatrix} + \begin{pmatrix} \cos\gamma_p & 0 & \sin\gamma_p \\ 0 & 1 & 0 \\ -\sin\gamma_p & 0 & \cos\gamma_p \end{pmatrix} \begin{pmatrix} 0 \\ 0 \\ \dot{\chi}_p \end{pmatrix} = \begin{pmatrix} -\dot{\chi}_p\sin\gamma_p \\ \dot{\gamma}_p \\ \dot{\chi}_p\cos\gamma_p \end{pmatrix} \tag{7}$$

The geometry relations in space can be described as

$$\mathbf{q} = \mathbf{p} + \mathbf{r} \tag{8}$$

It is also straightforward to compute the velocity of the vehicle in inertial frame

$$\frac{d\mathbf{q}}{dt}^I = \frac{d\mathbf{p}}{dt}^I + \frac{d\mathbf{r}}{dt}^I \tag{9}$$

Multiply both sides of equation (9) by rotate matrix R_I^F to get the expression

$$R_I^F \frac{d\mathbf{q}}{dt}^I = \frac{d\mathbf{p}}{dt}^F + \frac{d\mathbf{r}}{dt}^F + \omega_{F/I} \times \mathbf{r} \tag{10}$$

Meanwhile, we have $\frac{d\mathbf{q}}{dt}^I = \begin{pmatrix} \dot{x} & \dot{y} & \dot{z} \end{pmatrix}^T$, $\mathbf{r} = \begin{pmatrix} r_x & r_y & r_z \end{pmatrix}^T$, $\frac{d\mathbf{p}}{dt}^F = \begin{pmatrix} \dot{s} & 0 & 0 \end{pmatrix}^T$, $\frac{d\mathbf{r}}{dt}^F = \begin{pmatrix} \dot{r}_x & \dot{r}_y & \dot{r}_z \end{pmatrix}^T$, and $\omega_F \times \mathbf{r} = \begin{pmatrix} \dot{\gamma}_p r_z - \dot{\chi}_p \cos\gamma_p r_y \\ \dot{\chi}_p \cos\gamma_p r_x + \dot{\chi}_p \sin\gamma_p r_z \\ -\dot{\chi}_p \sin\gamma_p r_y - \dot{\gamma}_p r_x \end{pmatrix}$.

The error equation of the UAV can obtained

$$\begin{aligned}
\dot{r}_x &= V_g \cos\tilde{\chi}\cos\tilde{\gamma} - \dot{s} - \beta(s)\dot{s}r_z + \alpha(s)\dot{s}\cos(\gamma_p - \gamma)r_y \\
\dot{r}_y &= V_g \sin\tilde{\chi}\cos\tilde{\gamma} - \alpha(s)\dot{s}\cos\tilde{\gamma}r_x - \alpha(s)\dot{s}\sin(\gamma_p - \gamma)r_z \\
\dot{r}_z &= -V_g \sin\tilde{\gamma} - \alpha(s)\dot{s}\sin\tilde{\gamma}r_y - \beta(s)\dot{s}r_x \\
\dot{\tilde{\chi}} &= \dot{\chi}_p - \Gamma(\psi)\frac{g}{V_g}\tan\phi_c \\
\dot{\tilde{\gamma}} &= \dot{\gamma}_p - \alpha(\gamma_c - \gamma) = \dot{\gamma}_p - \alpha(\gamma_c - \gamma_p) - \alpha\tilde{\gamma}
\end{aligned} \tag{11}$$

where $\tilde{\chi} = \chi_p - \chi$ and $\tilde{\gamma} = \gamma_p - \gamma$.

We define the control inputs

$$\mathbf{u} = \begin{pmatrix} u_1 & u_2 & u_3 & u_4 & u_5 \end{pmatrix}^T = \begin{pmatrix} \cos\tilde{\chi} & \cos\tilde{\gamma} & \dot{s} & \tan\phi_c & \gamma_c \end{pmatrix}^T \tag{12}$$

The states of the system is selected

$$\mathbf{x} = \begin{pmatrix} x_1 & x_2 & x_3 & x_4 & x_5 \end{pmatrix}^T = \begin{pmatrix} r_x & r_y & r_z & \tilde{\chi} & \tilde{\gamma} \end{pmatrix}^T \tag{13}$$

It is obvious that

$$\begin{aligned}
\dot{x}_1 &= V_g u_1 u_2 - u_3 - \beta(s)u_3 x_3 + \alpha(s)u_3 u_2 x_2 \\
\dot{x}_2 &= V_g\sqrt{1-u_1^2}u_2 - \alpha(s)u_3 u_2 x_1 - \alpha(s)u_3\sqrt{1-u_1^2}x_3 \\
\dot{x}_3 &= -V_g\sqrt{1-u_2^2} - \alpha(s)u_3\sqrt{1-u_2^2}x_2 - \beta(s)u_3 x_1 \\
\dot{x}_4 &= \dot{\chi}_p - \Gamma(\psi)\frac{g}{V_g}u_4 \\
\dot{x}_5 &= \dot{\gamma}_p - \alpha u_5 + \alpha\gamma_p - \alpha x_5
\end{aligned} \tag{14}$$

Equation (14) can be expressed as

$$\frac{\partial \mathbf{x}}{\partial t} = A_f \mathbf{x} + B_f \mathbf{u}_f \tag{15}$$

where,

$$A_f = \begin{pmatrix} 0 & \alpha(s)u_3u_2 & -\beta(s)u_3 & 0 & 0 \\ -\alpha(s)u_2u_3 & 0 & -\alpha(s)u_3\sqrt{1-u_1^2} & 0 & 0 \\ -\beta(s)u_3 & -\alpha(s)u_3\sqrt{1-u_2^2} & 0 & 0 & 0 \\ 0 & 0 & 0 & 0 & 0 \\ 0 & 0 & 0 & 0 & -\alpha \end{pmatrix} \tag{16}$$

$$B_f = \begin{pmatrix} 1 & 0 & 0 & 0 & 0 \\ 0 & 1 & 0 & 0 & 0 \\ 0 & 0 & 1 & 0 & 0 \\ 0 & 0 & 0 & 1 & 0 \\ 0 & 0 & 0 & 0 & 1 \end{pmatrix} \tag{17}$$

$$\mathbf{u}_f = \begin{pmatrix} V_g u_1 u_2 - u_3 \\ V_g \sqrt{1-u_1^2} u_2 \\ -V_g \sqrt{1-u_2^2} \\ \dot{\chi}_p - \Gamma(\psi) \frac{g}{V_g} u_4 \\ \dot{\gamma}_p - \alpha u_5 + \alpha \gamma_p \end{pmatrix} \tag{18}$$

C. Integral LOS guidance

The integral LOS guidance for path following are usually employed in the guidance level where the goal is to prescribe a desired value for the course angle χ_d. Then, the control level tracks the given χ_d perfectly, such that ensure the performance of path following. According to the integral LOS guidance logic proposed in,[12] the desired course angle is:

$$\begin{aligned} \chi_d &= \chi_p - \tan^{-1}\left(\frac{r_y + \sigma r_{yin}}{\Delta}\right), \quad \Delta > 0 \\ \dot{r}_{yin} &= \frac{\Delta r_y}{(r_y + \sigma r_{yin})^2 + \Delta^2} \end{aligned} \tag{19}$$

where χ_p is the path tangential angle as defined in (3). r_y is the cross-tracking error and r_{yin} is the increment of the error. Δ is the lookahead distance and $\sigma > 0$ is an integral parameter. Both Δ and σ are constant parameters in the primary integral LOS guidance. Here, the desired course angle is employed as a reference angle for the vehicle to follow and the parameters are optimal selected in the MPC scheme.

D. linearized prediction models for the MPC

We introduce a time-varying function instead of constant parameters in (19). An additional freedom of selecting Δ can be employed to optimize the performance of path following.

The closed-loop system is explained as follows.

$$\begin{aligned} \frac{\partial \mathbf{x}}{\partial t} &= A_f \mathbf{x} + B_f \mathbf{u}_f \\ \dot{\Delta} &= \mu \end{aligned} \tag{20}$$

where μ is an additional control input that we introduce to optimize the lookahead distance.

We redefined the state $\mathbf{x}_l = [\ \mathbf{x} \quad \Delta\ ]^T$ and control input $\mathbf{u}_l = [\ \mathbf{u}_f \quad \mu\ ]^T$.

The modified closed-loop system is:

$$\frac{\partial \mathbf{x}_l}{\partial t} = A_l \mathbf{x}_l + B_l \mathbf{u}_l \tag{21}$$

where

$$A_l = \begin{pmatrix} 0 & \alpha(s) u_3 u_2 & -\beta(s) u_3 & 0 & 0 & 0 \\ -\alpha(s) u_2 u_3 & 0 & -\alpha(s) u_3 \sqrt{1-u_1^2} & 0 & 0 & 0 \\ -\beta(s) u_3 & -\alpha(s) u_3 \sqrt{1-u_2^2} & 0 & 0 & 0 & 0 \\ 0 & 0 & 0 & 0 & 0 & 0 \\ 0 & 0 & 0 & 0 & -\alpha & 0 \\ 0 & 0 & 0 & 0 & 0 & 0 \end{pmatrix} \tag{22}$$

$$B_l = \begin{pmatrix} 1 & 0 & 0 & 0 & 0 & 0 \\ 0 & 1 & 0 & 0 & 0 & 0 \\ 0 & 0 & 1 & 0 & 0 & 0 \\ 0 & 0 & 0 & 1 & 0 & 0 \\ 0 & 0 & 0 & 0 & 1 & 0 \\ 0 & 0 & 0 & 0 & 0 & 1 \end{pmatrix} \tag{23}$$

ϕ_c, γ_c and Δ satisfy the following constraints

$$\begin{aligned} -30^\circ &\leq \phi_c \leq 30^\circ \\ -10^\circ &\leq \gamma_c \leq 10^\circ \\ 15m &\leq \Delta \leq 45m \end{aligned} \tag{24}$$

III. Control Scheme

We aim at minimizing the convergence time to the path and simultaneously reducing the possible overshoots, while preserving the closed-loop stability. The integral LOS control scheme presented in the previous studies has different performance depending on the choice of Δ. Small value of Δ results in fast convergence but large overshoots to the path. On the contrary, large value of Δ results in little overshoots but slow convergence. A time-varying Δ is introduced to overcome the drawback of constant value of Δ.

First, the linearized system (21) can be written as the discrete form

$$\mathbf{x}(k+1) = A\mathbf{x}(k) + B\mathbf{u}(k) \tag{25}$$

where $A = I + A_l T_s, B = B_l T_s$. T_s is the sampling time.

Assuming that at the sampling instant $k, k > 0$, the state variable vector $\mathbf{x}(k)$, which provides the current plant information, is available through measurements. The future control trajectory is denoted by

$$U(k) = [\mathbf{u}^T(k|k), \mathbf{u}^T(k+1|k), \ldots, \mathbf{u}^T(k+N_c-1|k)] \tag{26}$$

where N_c is called the control horizon dictating the number of parameters used to capture the future control trajectory. The future state variables are predicted for N_p number of samples, where N_p is the prediction horizon, and N_p is also the length of the optimization window. We denote the future state variables as

$$X(k) = [\mathbf{x}^T(k+1|k), \mathbf{x}^T(k+2|k), \ldots, \mathbf{x}^T(k+N_p|k)] \tag{27}$$

Here, the control horizon N_c is selected to be less than (or equal to) the prediction horizon N_p.

The future state variables are calculated sequentially using the set of future control parameters:

$$\mathbf{x}(k+1|k) = A\mathbf{x}(k|k) + B\mathbf{u}(k|k) \tag{28}$$

$$\mathbf{x}(k+2|k) = A\mathbf{x}(k+1|k) + B\mathbf{u}(k+1|k) = A^2\mathbf{x}(k|k) + AB\mathbf{u}(k|k) + B\mathbf{u}(k+1|k) \tag{29}$$

$$\mathbf{x}(k+N_p|k) = A^{N_p}\mathbf{x}(k|k) + A^{N_p-1}B\mathbf{u}(k|k) + A^{N_p-2}B\mathbf{u}(k+1|k) + \cdots + A^{N_p-N_c}B\mathbf{u}(k+N_c-1|k) \tag{30}$$

It can be shown that

$$X(k) = F(k)\mathbf{x}(k|k) + \phi(k)U(k) \tag{31}$$

where

$$F(K) = [a(k+1,k), a(k+2,k), \ldots, a(k+N_p,k)]^T \tag{32}$$

$$\phi(k) = \begin{pmatrix} b_{11}(k) & 0 & \cdots & 0 \\ b_{21}(k) & b_{22}(k) & \cdots & \vdots \\ \vdots & \vdots & \ddots & \vdots \\ b_{N_p1}(k) & b_{N_p2} & \cdots & b_{N_pN_p}(k) \end{pmatrix} \tag{33}$$

with $a(i,j)$ and $b_{ij}(k)$ are defined as

$$a(i,j) = \begin{cases} I, & \text{if} \quad i = j \\ \prod_{i=0}^{N_p-1} A(k+i), & \text{if} \quad i > j \end{cases} \tag{34}$$

$$b_{ij}(k) = a(i,j)B \tag{35}$$

where the double subscript notation $(k+j|k)$ denotes the prediction made at time k of a value at time $k+j$.

According to the standard MPC method. At time k, the quadratic cost function can be considered

$$\begin{aligned} J(k) &= \sum_{j=1}^{N} \{\mathbf{x}^T(k+j|k)Q\mathbf{x}(k+j|k) + \mathbf{u}^T(k+j-1|k)R\mathbf{u}(k+j-1|k) \\ &= X^T(k)\hat{Q}X(k) + U^T(k)\hat{R}U(k) \\ &= (F(k)\mathbf{x}(k|k) + \phi(k)U(k))^T\hat{Q}(F(k)\mathbf{x}(k|k) + \phi(k)U(k)) + U^T(k)\hat{R}U(k) \\ &= (F(k)\mathbf{x}(k|k))^T\hat{Q}((F(k)\mathbf{x}(k|k)) + 2(\phi(k)U(k))^T\hat{Q}F(k)\mathbf{x}(k|k) + U^T(k)(\hat{R} + \phi^T(k)\hat{Q}\phi(k))U(k) \\ &= (F(k)\mathbf{x}(k|k))^T\hat{Q}((F(k)\mathbf{x}(k|k)) + \overbrace{2(\phi(k)U(k))^T\hat{Q}F(k)\mathbf{x}(k|k))} \\ &\quad + \overbrace{U^T(k)((\hat{R} + \phi^T(k)\hat{Q}\phi(k))U(k) + ((F(k)\mathbf{x}(k|k))^T\phi(k)\hat{Q})(\hat{R} + \phi^T(k)\hat{Q}\phi(k))^{-1}\hat{Q}^T\phi^T(k)F(k)\mathbf{x}(k|k))} \\ &\quad - (F(k)\mathbf{x}(k|k))^T\phi(k)\hat{Q})(\hat{R} + \phi^T(k)\hat{Q}\phi(k))^{-1}\hat{Q}^T\phi^T(k)F(k)\mathbf{x}(k|k) \end{aligned} \tag{36}$$

where $Q > 0$ and $R > 0$ are the weighting matrices. The quantities under the $\overbrace{\cdot}$ are the completed squares. We introduce a new function

$$J^* = \{[\hat{R} + \phi^T(k)\hat{Q}\phi(k)]U(k) - \phi^T(k)\hat{Q}F(k)\mathbf{x}(k|k)\}^T\{[\hat{R} + \phi^T(k)\hat{Q}\phi(k)]U(k) - \phi^T(k)\hat{Q}F(k)\mathbf{x}(k|k)\} \tag{37}$$

Since the first and last terms in (36) are independent of the variable $U(k)$. The minimum of the cost function $J(k)$ is achieved if the quantity J^* equals zero, and this can be easily verified by opening the squares. Then we can obtain the optimal solution

$$U(k) = (\hat{R} + \phi^T(k)\hat{Q}\phi(k))^{-1}\phi^T(k)\hat{Q}\mathbf{x}(k|k) = H^{-1}(k)S(k) \tag{38}$$

where $H(k) = \hat{R} + \phi^T(k)\hat{Q}\phi(k)$ is a Hessian matrix and it is always positive definite with $Q > 0$ and $R > 0$.

This study describes the effect of optimal parameters of integral LOS and the stability of the MPC is guaranteed by using a prediction horizon, which is distinctly illustrated.[17]

IV. Experiment

To verify the effectiveness and applicability of the proposed control strategy, we developed a high-fidelity semi-physical experiment scheme. The proposed approach has been tested with an X-plane environment, which provides very accurate aircraft models and has the possibility of exchanging data with external systems. The aircraft models that are employed in the X-plane are based on the exact physical model and material.

We use the X-plane to provide the exact physical model and material of the UAV in the experiment; the X-plane can be used to establish the flight environment conditions. As shown in Fig. 2, the conditions of the flight environment can be established. The majority of the conditions are independent to our work, and the wind and turbulence are established in the low-altitude layer (below 2000 feet). In the figure, the disk with four arrows is used to establish the direction of the wind, and the speed of wind are set in the first bar with the unit kt (1kt = 0.514 m/s).

A. Predefined Path

Based on the distance, orientation and curvature, smooth curvature profiles can be easily provided. In particular, double continuous curvature (DCC) paths, which consist of a combination of clothoids, line segments and arcs, are extensively employed. Some practical applications, such as obstacle avoidance, differ from cruising or investigation because the change in curvature and orientation is acute and unexpected.

In actual flight applications, the flight paths are determined by a sequence of waypoints from the ground station. To obtain a continuous and non-constant curvature path, we employ a B-spline to produce paths that pass through the

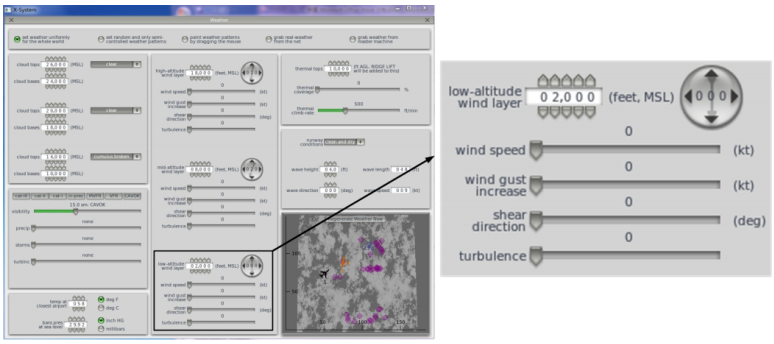

Figure 2. Environment set page of the X-plane.

predefined waypoints and a continuous curvature of paths. A B-spline curve $S : [0, 1] \rightarrow R^2$ is defined as

$$S(u) = \sum_{i=0}^{m} P_i N_{i,p}(u) \tag{39}$$

where, P_i is the control point. $N_{i,p}(u)$ is defined by the Cox-de Boor iterative formula

$$\begin{aligned} N_{i,0}(u) &= \begin{cases} 1, & if \quad u_i \le u \le u_{i+1} \\ 0, & otherwise \end{cases} \\ Ni, p(u) &= \frac{u-u_i}{u_{i+p}-u_i} N_{i,p-1}(u) + \frac{u_{i+p+1}-u}{u_{i+p+1}-u_{i+1}} N_{i+1,p-1}(u) \end{aligned} \tag{40}$$

where u_i denotes knots, and $u_0 \le u_1 \le \cdots \le u_m$. The number of knots is $m + 1$, $U = [u_0, u_1, \ldots, u_m]$ is a knot vector, and p is the degree of the basic function. We define $p = 3$ in our experiments.

B. Platform

The entire system consists of three segments *ground control station*, *autopilot* and *X-plane* as shown in Fig. 3. The ground control station is developed and employed to communicate with the X-plane by User Datagram Protocol (UDP) communication. The autopilot and computer are connected with a network cable, which simulates a wireless transceiver. The X-plane provides all movement states to autopilot and simultaneously receives control commands. The ground control station is employed to record and present the flight procedure.

The autopilot, which is developed by our work group, uses the position, orientation, heading angle, and other information about the UAV to calculate the low-level control signals. We employ an active disturbance rejection control (ADRC) method to implement the inner-loop control, and the ADRC was proposed to address the nonlinear systems with uncertain dynamics and disturbances. The framework of the ADRC consists of two segments: the first segment involves observation to compensate for the uncertainties and the second segment involves regulation of the desired performances of the compensated system.

The *Autopilot*, with its hardware and embedded software, and the *Ground station*, are both developed by our group. The main characters of the *Autopilot* are with

- Two Cortex-M4 ARM: 168MHz;
- Double 100M network interfaces;
- Supporting data record by SD card;
- 8M SRAM, 6 UART, 3 SPI, 2 CAN, and 16 AD conversion with 12 bits.

The *Great Planes PT-60 RC plane* is used in the experiments. The frame of the plane and its main parameters are shown in Fig. 4

The aircraft has a traditional configuration, and the desired curved path is generated by cube spline interpolation. Consider eight waypoints in Table 1, where Lon and Lat are the longitude and the latitude, respectively.

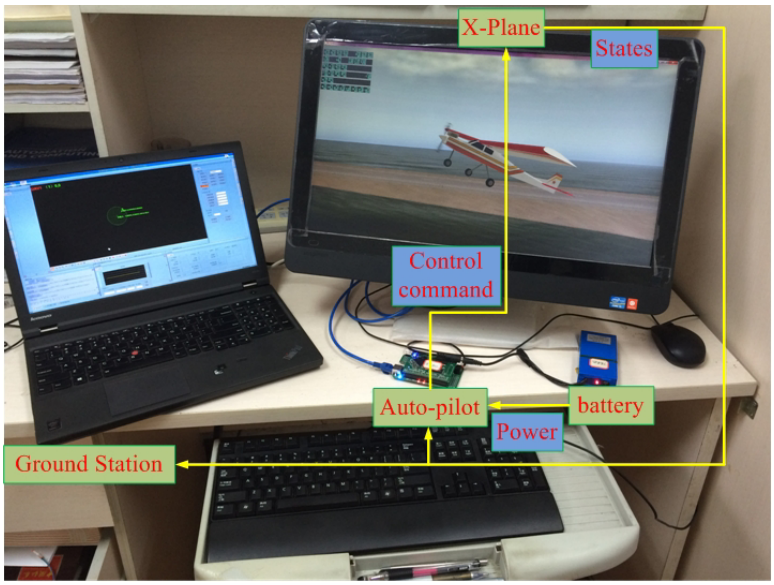

Figure 3. High-fidelity semi-physical experiment environment, constructed by an actual autopilot, ground station and the X-Plane.

Figure 4. Great Planes PT-60 RC plane, and its main parameters in the X-Plane flight simulator.

Table 1. Positions of waypoints

Waypoint	WP1	WP2	WP3	WP4	WP5	WP6	WP7	WP8	WP9
Lon(deg)	124.3174	124.3133	124.3174	124.3209	124.3252	124.3291	124.3252	124.3209	124.3174
Lat(deg)	48.2733	48.2674	48.2610	48.2636	48.2610	48.2674	48.2732	48.2709	48.2733
x(m)	0	-656.05	-1367.7	-1078.6	-1367.7	-656.07	-11.12	-266.87	0
y(m)	0	303.44	0	-259.03	-577.28	-865.93	-577.27	-259.03	0
Altitude(m)	100	120	100	120	100	120	100	120	100

C. Results

The parameters in control scheme are shown in Table 2:

Table 2. Parameters of control scheme

Parameter	Value	Range
Q	diag(0.1,1,0.5,1,0.2,1)	-
R	diag(1,1,1,1,1,1)	-
V_g	15 m/s	12-18 m/s
W	5 m/s	3-7 m/s
Δ	30 m	15-45 m
σ	1.5	1-2
α	0.5	0.1-1
Experiment time	300 s	-
Sampling time	0.1 s	-
$N_P = N_c$	10	-

The tracking performance of the proposed control scheme is shown in Fig. 5, and it illustrates the ability of the UAV to follow a curved path with acute angles. The constant airspeed of the UAV is 15 m/s. The wind speed ranges from 3 m/s to 7 m/s from 90 degrees southwest, which indicates that the wind speed accounts for 20% to 50% of the airspeed of the UAV. The red curve represents the desired path, and the blue line represents the flight path. Although the transitions in the corner points exhibit some lateral following errors, the arc of the flown path and the desired are coincide.

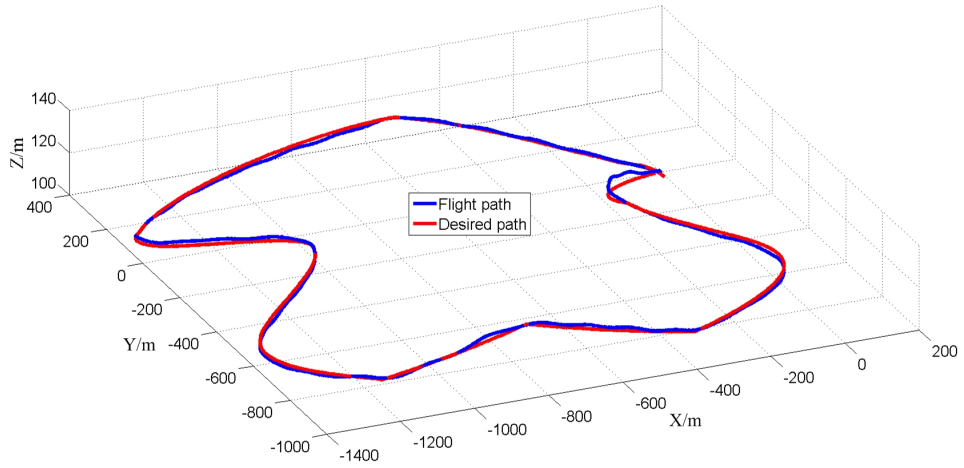

Figure 5. Tracking performance of the UAV

The tracking performance and error of different lookahead distances (Δ=15 m, Δ=45 m and variable Δ) are shown in Fig. 6 and Fig. 7, respectively. When the curvature of the desired path is slowly altered, the tracking error of three types of Δ are similar. Conversely, if the curvature of the desired path is rapidly altered, the tracking error of constant Δ is much larger than the tracking error of variable Δ. It is clear that our proposed control scheme has a better tracking performance for a general curved path.

For a given group of parameters, we define the $u(t)$ and $e(t)$ as the control input and tracking error at time t. The total control inputs and tracking errors are defined as

$$\begin{aligned} \Sigma|U|^2 &= \sum_{t=0}^{t=T} u(t)^2 \\ \Sigma|E|^2 &= \sum_{t=0}^{t=T} e(t)^2 \end{aligned} \tag{41}$$

The error and control of different value of lookahead distances are shown in Table 3. It is obvious that variable Δ combines the advantage of small and large value of Δ simultaneously. The control input and tracking error are both

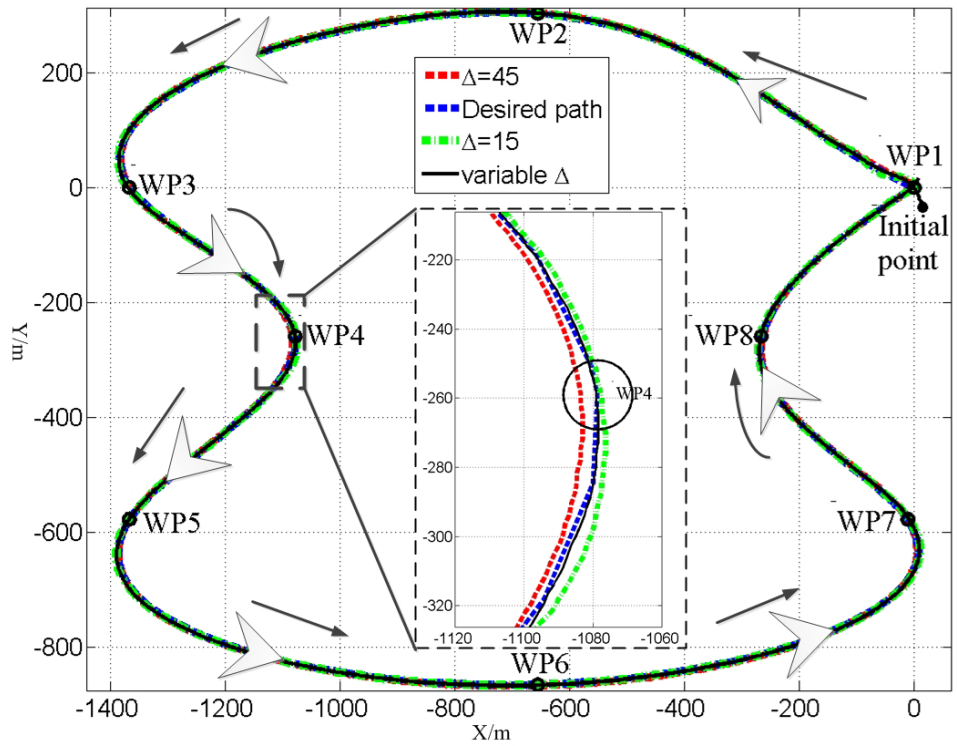

Figure 6. Tracking results of the UAV in two dimensions plane

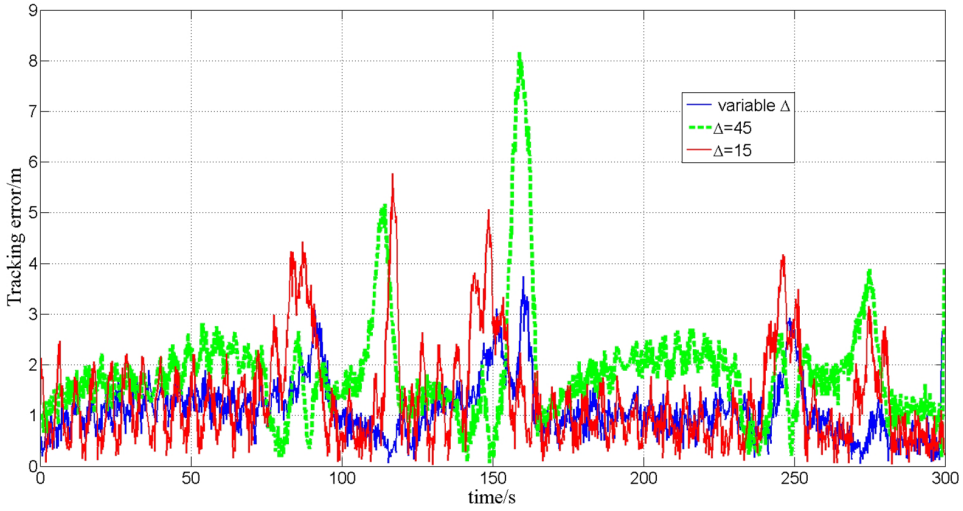

Figure 7. Tracking error of the UAV

smaller than the two fixed Δ in the experiments.

Table 3. The error and control of different value of lookahead distances

Δ(m)	$\Sigma\|E\|^2(m)$	$\Sigma\|U\|^2(rad/s)$	Max$\|e(t)\|$ (m)	Mean$\|e(t)\|$ (m)
15	1972	1460.4	5.86	1.436
variable	1726.1	1837.9	3.52	1.106
45	2592	3403.9	8.37	2.4

V. Conclusion

In this paper we discussed a curved path following strategy that combines integral line-of-sight (LOS) guidance logic and the model predictive control (MPC) approach to ensure a small fixed-wing unmanned aerial vehicle (UAV) converging to the desired curved path with input constraints. There is a tradeoff that large lookahead distance will lead to fast convergence and large overshoots, and small lookahead distance will lead to slow convergence and minor overshoots. To obtain a combination of fast convergence and minor overshoots compared with the constant lookahead LOS algorithms, a modified MPC scheme integrated with the integral LOS guidance logic is proposed to generate an optimal lookahead distance along the error model of the UAV defined in Frenet-Serret frame with control constraints are considered explicitly. A high-fidelity semi-physical experiment scheme is developed to verify the effectiveness and applicability of the proposed control strategy.

Acknowledgment

This work was supported by National Natural Science Foundation of China (61403406).

References

[1]Ostertag, E., "An Improved Path-Following Method for Mixed Controller Design," *IEEE Transactions on Automatic Control*, Vol. 53, No. 8, 2008, pp. 1967–1971.

[2]Aguiar, A. P., Hespanha, J. P., and Kokotović, P. V., "Performance limitations in reference tracking and path following for nonlinear systems," *Automatica*, Vol. 44, No. 3, 2008, pp. 598–610.

[3]Park, S., Deyst, J., and How, J. P., "Performance and Lyapunov stability of a nonlinear path following guidance method," *Journal of Guidance, Control, and Dynamics*, Vol. 30, No. 6, 2007, pp. 1718–1728.

[4]Morro, A., Sgorbissa, A., and Zaccaria, R., "Path following for unicycle robots with an arbitrary path curvature," *IEEE Transactions on Robotics*, Vol. 27, No. 5, 2011, pp. 1016–1023.

[5]Beard, R. W., Ferrin, J., and Humpherys, J., "Fixed wing UAV path following in wind with input constraints," *IEEE Transactions on Control Systems Technology*, Vol. 22, No. 6, 2014, pp. 2103–2117.

[6]Brezoescu, C. A., Espinoza, T., Castillo, P., and Lozano, R., "Adaptive trajectory following control of a fixed-wing UAV in presence of crosswind," *International Conference on Unmanned Aircraft Systems (ICUAS'12)*, 2012, pp. Proceedings–of.

[7]Gonçalves, V. M., Pimenta, L. C., Maia, C. A., Dutra, B. C., and Pereira, G. A., "Vector Fields for Robot Navigation Along Time-Varying Curves in-Dimensions," *IEEE Transactions on Robotics*, Vol. 26, No. 4, 2010, pp. 647–659.

[8]Shiriaev, A., Perram, J. W., and Canudas-de Wit, C., "Constructive tool for orbital stabilization of underactuated nonlinear systems: Virtual constraints approach," *IEEE Transactions on Automatic Control*, Vol. 50, No. 8, 2005, pp. 1164–1176.

[9]Arogeti, S. A. and Berman, N., "Path following of autonomous vehicles in the presence of sliding effects," *IEEE Transactions on Vehicular Technology*, Vol. 61, No. 4, 2012, pp. 1481–1492.

[10]Calvo, O., Rozenfeld, A., Souza, A., Valenciaga, F., Puleston, P. F., and Acosta, G., "Experimental results on smooth path tracking with application to pipe surveying on inexpensive AUV," *2008 IEEE/RSJ International Conference on Intelligent Robots and Systems*, IEEE, 2008, pp. 3647–3653.

[11]Zheng, Z., Guo, W., and Wu, Z., "Direct-adaptive fuzzy path following control for an autonomous airship," *Control Decision*, Vol. 29, No. 3, 2014, pp. 418–424.

[12]Borhaug, E., Pavlov, A., and Pettersen, K. Y., "Integral LOS control for path following of underactuated marine surface vessels in the presence of constant ocean currents," *Decision and Control, 2008. CDC 2008. 47th IEEE Conference on*, IEEE, 2008, pp. 4984–4991.

[13]Caharija, W., Candeloro, M., Pettersen, K. Y., and Sørensen, A. J., "Relative velocity control and integral LOS for path following of underactuated surface vessels," *IFAC Proceedings Volumes*, Vol. 45, No. 27, 2012, pp. 380–385.

[14]Oh, S.-R. and Sun, J., "Path following of underactuated marine surface vessels using line-of-sight based model predictive control," *Ocean Engineering*, Vol. 37, No. 2, 2010, pp. 289–295.

[15]Lekkas, A. M. and Fossen, T. I., "Integral LOS path following for curved paths based on a monotone cubic Hermite spline parametrization," *IEEE Transactions on Control Systems Technology*, Vol. 22, No. 6, 2014, pp. 2287–2301.

[16]Fossen, T. I., Pettersen, K. Y., and Galeazzi, R., "Line-of-sight path following for dubins paths with adaptive sideslip compensation of drift forces," *IEEE Transactions on Control Systems Technology*, Vol. 23, No. 2, 2015, pp. 820–827.

[17]Marjanovic, O. and Lennox, B., "Infinite horizon model predictive control with no terminal constraint," *Computers & chemical engineering*, Vol. 28, No. 12, 2004, pp. 2605–2610.